scientific reports

Check for updates

OPEN

MoSeq based 3D behavioral profiling uncovers neuropathic behavior changes in diabetic mouse model

Akm Ashiquzzaman[1,8], Eunbin Lee[1,8], Brahnu Fentaw Znaub[1,2,8], An Nazmus Sakib[1], Geehoon Chung[3,4], Sang Seong Kim[1], Young Ro Kim[5,6], Hyuk-Sang Kwon[1,7]✉ & Euiheon Chung[1,7]✉

Diabetic neuropathy (DN) is a prevalent and debilitating complication of diabetes, significantly impairing quality of life through chronic pain, sensory deficits, and motor dysfunction. Despite its widespread impact, current rodent behavioral assessments using 2D tracking methods primarily quantify basic locomotion, such as distance and speed, but lack resolution to detect subtle, pattern-based motor impairments characteristic of DN. This study employed MoSeq-based 3D behavioral profiling combined with unsupervised machine learning to identify subtle yet significant alterations in nicotinamide (NA)- and streptozotocin (STZ)-induced DN mouse models. Our analysis identified 22 distinct behavioral syllables, with DN mice exhibiting increased stress-associated behaviors such as head weaving, wall jumping, and nasal hesitancy, while displaying decreased locomotor activities including walking and rearing. These alterations were accompanied by heightened mechanical sensitivity indicative of neuropathic pain and a more predictable, less exploratory behavioral transition pattern, suggesting a restricted behavioral repertoire rather than improved motor coordination. Additionally, MoSeq-based profiling enabled detailed analysis of movement organization and temporal transitions, highlighting stereotyped behavioral sequences and notably decreased exploratory behaviors in DN mice. These behavioral patterns indicate that DN-associated pain is more strongly related to impairments in behavioral adaptability and higher-order motor planning than to simple reductions in movement, suggesting underlying dysfunctions in sensorimotor or cognitive control circuits. These findings indicate that MoSeq can be used as a valuable tool for high-resolution behavioral quantification in diabetic neuropathic animal pain model, enabling refined evaluation of neuropathic phenotypes and therapeutic efficacy in preclinical studies.

Diabetes is a metabolic disorder characterized by high blood glucose levels. According to the International Diabetes Federation (IDF), the number of adults with diabetes is projected to increase from 463 million in 2021 to 783 million by 2045, a 46% rise[1]. This makes it the largest global epidemic of the twenty-first century[2]. While diabetes can potentially affect multiple organs including the eyes, heart, kidneys, and nerves, approximately 60% of patients with diabetes develop diabetic peripheral neuropathy[3]. In particular, diabetic neuropathy (DN) is characterized by severe and intractable pain, sensory loss, and motor function impairment with considerable morbidity, and drastically diminished quality of life[4,5]. The pathophysiology of DN remains poorly understood[6], and investigating how behavioral changes relate to DN-associated symptoms and disease markers may offer important insights for the development of effective therapeutic strategies. In this context, DN animal models provide a critical platform for the quantitative monitoring of disease-related changes in behavior and physiology,

[1]Department of Biomedical Science and Engineering, Gwangju Institute of Science and Technology, Gwangju, South Korea. [2]Department of Biomedical Science and Engineering, University of NE–Lincoln, Lincoln, NE, USA. [3]Neurogrin Inc., Seoul, South Korea. [4]Department of Physiology, College of Medicine, Chungbuk National University, Cheongju, Republic of Korea. [5]Department of Radiology, Harvard Medical School, Boston, MA, USA. [6]Athinoula A. Martinos Center for Biomedical Imaging, Massachusetts General Hospital, Charlestown, MA, USA. [7]AI Graduate School, Gwangju Institute of Science and Technology, Gwangju, South Korea. [8]Akm Ashiquzzaman, Eunbin Lee and Brahnu Fentaw Znaub contributed equally to this work. ✉email: hyuksang@gist.ac.kr; ogong50@gist.ac.kr

both of which are essential for evaluating therapeutic outcomes and characterizing the trajectory of neuropathic progression.

To evaluate these changes, various quantitative methods such as nerve conduction analysis, histopathological analysis, biochemical analysis, and behavioral tests have been employed in the assessment of DN[7–11]. Among these, behavioral tests are the most widely used method for evaluating the impact of neuropathy on sensory, cognitive, motor, and coordination functions in rodents. This is particularly relevant in light of clinical evidence showing that individuals with DN commonly exhibit sensory deficits and motor dysfunctions such as changes in gait and balance[12,13], which reflect underlying functional impairments. Although rodent models may not fully replicate these clinical features, behavioral assessments remain essential for capturing subtle alterations in motor behavior and sensory function.

Moreover, several studies have demonstrated a reduced range of motion at both the ankle[14,15] and knee joints[16]. Accordingly, the evaluation of locomotor and exploratory activities in rodent models, particularly using the open-field test (OFT), has been frequently employed to assess motor functions and measure treatment efficacy[17–24]. For example, the effects of various treatments such as melatonin[25], heat shock protein 90 inhibition[20], Nitecapone[22], Angipars[24], and octreotide as a neuroprotective agent[23] on locomotor and exploratory behaviors have been studied in rat DN models. These studies quantified parameters like rearing frequency, crossed segments, grooming, speed, time spent in motion, and total distance traveled.

However, these methods have significant limitations. Traditional two-dimensional (2D) tracking methods cannot capture the subtle nuances of rodent behavior, especially the intricate movements and postural changes that occur in three dimensions. As a result, complex sequences of behavior, known as higher-order behavioral motifs[26–28], are often missed by 2D analysis. This limits our understanding of the full range of behavioral changes associated with DN. Moreover, early-stage or mild behavioral changes may go undetected due to the lack of sensitivity of 2D methods, hindering early diagnosis and the evaluation of treatment effectiveness.

Given these limitations, there is a clear need for more advanced analytical techniques that can capture the full complexity of rodent behavior in three dimensions. Recent advances in machine vision and unsupervised learning have enabled more sophisticated approaches to capturing the complexity of rodent behavior. Motion Sequencing (MoSeq) leveraging these advancements enables the analysis of behavioral transition matrices, providing insights into movement flow and sequence predictability beyond isolated behavioral feature extraction. Additionally, Auto-Regressive Hidden Markov Models (AR-HMMs) facilitate the detection of latent motor states using behavioral data extracted by MoSeq, uncovering dynamic shifts in movement that conventional locomotor assessments often miss.

Finally, we hypothesize that the MoSeq framework can reveal behavioral signatures of DN that may be overlooked by conventional 2D tracking methods. These findings could provide valuable insights into how neuropathic pain affects motor control and adaptive behavior, offering a novel approach for evaluating therapeutic efficacy and improving treatment strategies in preclinical models.

Materials and methods

Animals

The handling of animals was conducted in accordance with the guidelines of the Institutional Animal Care and Use Committee board (IACUC) of the Gwangju Institute of Science and Technology (GIST), South Korea. Experimental protocols were approved by the Laboratory Animal Resource Center (LARC) at GIST under protocol #GIST-2024-028. The study utilized 12 male C57BL/6 mice, aged between 5 and 6 weeks and weighing 25–30 g on average. The mice were obtained from Damul Science (Daejeon, Republic of Korea). After the completion of the experiments, the mice were sacrificed using a humane euthanasia method in compliance with IACUC guidelines. Carbon dioxide (CO_2) euthanasia was performed in a dedicated chamber the gradual displacement of air, followed by cervical dislocation to ensure death. This procedure was conducted to minimize suffering, adhering to the AVMA Guidelines for the Euthanasia of Animals (2020). The study is reported in accordance with the ARRIVE guidelines (https://arriveguidelines.org), ensuring transparency and rigor in the design, conduct, and reporting of the animal experiments.

Nicotinamide and streptozotocin-induced diabetes

Type-2 diabetes was induced following established protocols[29,30], using mice (n = 4 in the control group and n = 8 in the experimental group). Diabetes induction in the experimental group commenced with the intraperitoneal administration of nicotinamide (NA) solution at a dosage of 240 mg/kg. After a 15-min interval, the experimental group received an intraperitoneal injection of streptozotocin (STZ) solution at a dosage of 100 mg/kg. Simultaneously, mice in the control group were administered an equivalent volume of citrate buffer (pH 4.5) via intraperitoneal injection. Confirmation of diabetes induction involved assessing blood glucose level two weeks post-NA + STZ injection using commercial kits (One Touch Basic blood glucose monitoring system), while body weight was measured using a digital analytical balance. The onset of diabetic painful neuropathy was evaluated two weeks after NA and STZ injections by testing the mice's sensitivity to mechanical stimuli (see Fig. 1A).

Assessment of mechanical sensitivity

Mechanical sensitivity was assessed using von Frey filaments, adhering to the established protocol[31]. Mice were acclimated for one hour in cages with a mesh or barred floor before testing. The von Frey filaments, starting with the 0.16-g filament, were applied to the plantar surface of the hind paw until a paw withdrawal response was observed, and the corresponding force value was recorded. Baseline measurements were taken prior to diabetes induction, providing a reference for subsequent evaluations. Significantly reduced hind paw mechanical

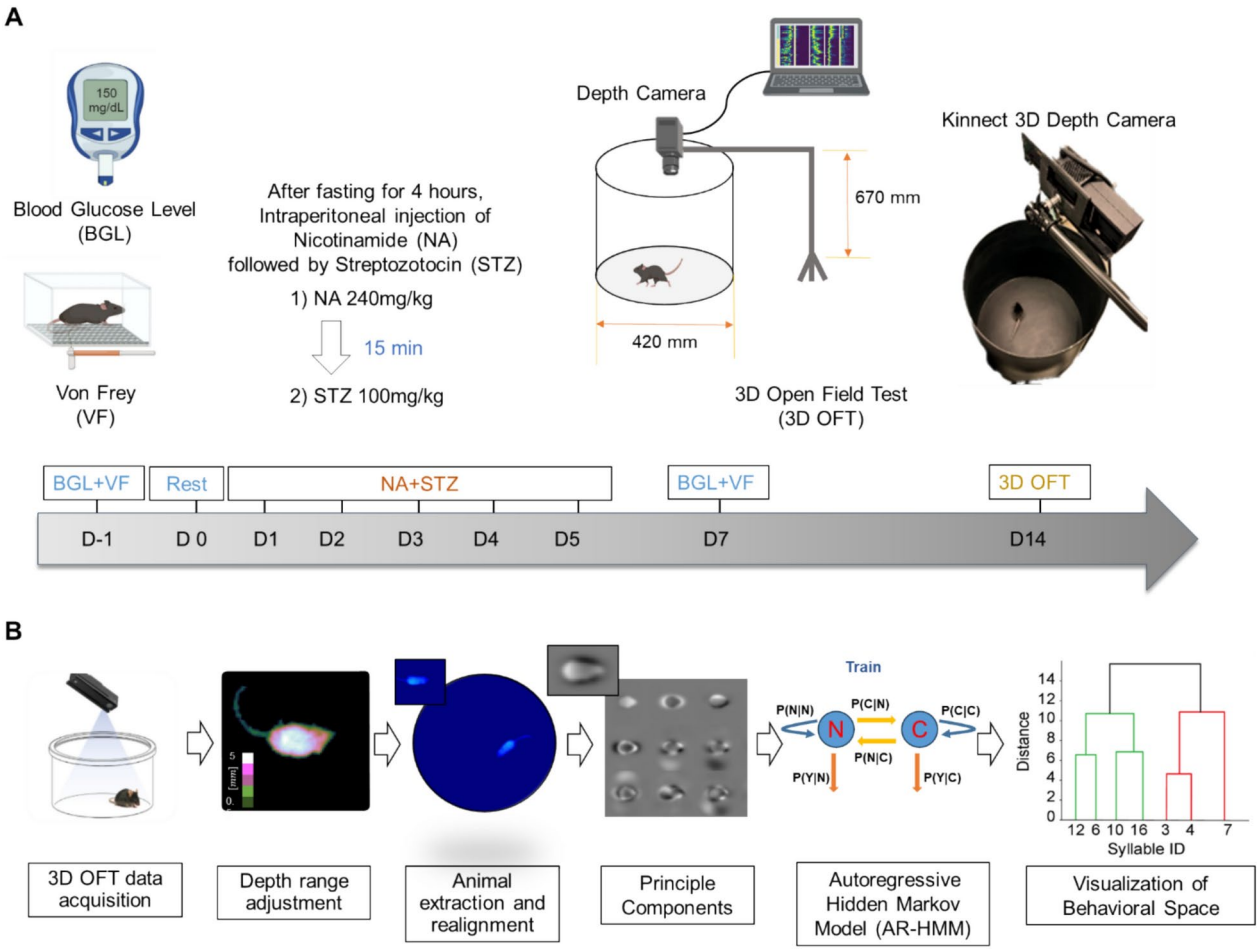

Fig. 1. Experimental workflow and setup. (**A**) Baseline assessments, including the von-Frey filament test, weight measurement, and blood glucose level evaluation, were conducted. In week one, animals underwent an intraperitoneal injection (i.p.) of nicotinamide (240 mg/kg), streptozotocin (STZ) (100 mg/kg) and citrate buffer. Week 2 involved the measurement of blood glucose levels and weight. Diabetic neuropathy development was assessed at the end of week two using the von-Frey filament test. Additionally, the Circular Open Field Test was conducted in week three. The figure was created with BioRender.com. The experimental setup is depicted, showcasing a circular open field test (photo), a drawing of the open field with a depth camera, and real-time imagery with a mouse. (**B**) Mouse 3D pose dynamics were recorded using a depth camera positioned above the arena. Subsequent steps included arena detection for data extraction and modeling, involving principal component analysis and fitting an Auto Regressive Hidden Markov Model (AR-HMM). The data were then fed into an analysis and visualization tool, encompassing interactive syllable labeling, computation of syllable statistics, and visualization of syllable transition frequencies.

withdrawal thresholds were considered indicative of mechanical allodynia, offering insights into neuropathic pain sensitivity in the experimental mouse model.

Open field test recording

Mice were maintained under standard animal facility conditions, with a temperature of 25 ± 3 °C and a relative humidity of 50 ± 15%. Upon introduction into the colony at 5 weeks of age, the mice were group-housed in a reverse 12-h light/12-h dark cycle. On the day of testing, mice were transported to the laboratory in a light-tight container. They underwent a 10-min habituation period in cages with fresh bedding, with ad libitum access to food and water, within the experimental room. Following habituation, the mice were placed in the center of a circular 16.5″-diameter open-field arena (OFA) enclosure with a height of 14.2″. A 5-min habituation period allowed the mice to acclimate to the field before initiating a 30-min experimental period, during which video recording took place (see Fig. 1B).

Open Field Test (OFT) Recording of each mouse (n = 4 control, n = 8 DN) underwent three independent OFT sessions to enhance behavioral profiling and reduce trial-to-trial variability. Recordings were conducted under identical conditions across sessions, ensuring robust assessment of locomotor and exploratory behaviors. All experiments were conducted under infrared light conditions. After each experiment, the enclosure was cleaned

with 70% ethanol before reuse. The data acquisition process mirrored previous descriptions[32], employing three parallel setups for increased throughput.

Mice were tracked in 3D using a Kinect for Windows v1 (Microsoft), projecting structured infrared light onto the imaging field. A boom tripod (Manfrotto) maintained a stable top-down view of the mouse within the recording arena. Figure 1A details the setup process. The Kinect v1, with a minimum working distance of 0.5 m (in near mode), was positioned optimally between 0.6 and 0.75 m depending on ambient light conditions and assay material. Data from the Kinect were transmitted to a custom-built acquisition computer (48 GB RAM, Intel i7 CPU, 512 GB SSD) via USB.

A custom MATLAB script interfaced with the Kinect through the official Microsoft.NET API, capturing depth frames at a rate of 30 frames per second and saving them in raw binary format (16-bit unsigned integers) to disk. Experimental metadata, including mouse group and session trial, were captured and stored in the same folder as the raw binary depth data.

Following the experiment, a specified region of interest delineated the mouse's feasible exploration area, which was saved alongside the depth data to simplify subsequent data extraction by eliminating pixels outside the arena. Figure 1B details the data processing steps for Motion Sequencing (MoSeq).

Data preprocessing and extraction

The extraction software used in this study was implemented in Python, leveraging key libraries such as MPI4Py, H5Py, joblib, pandas, OpenCV, Scikit-Learn, Scikit-Image, MoviePy, and SciPy. To extract and align 3D representations of the mouse from raw depth video data, each frame was first read as a rectilinear block of unsigned 16-bit integers. These values were converted into millimeter-scale depth measurements through a right-bit shift operation (by three places). Background subtraction was performed by computing a reference background image, obtained as the median depth of the first 1,000 frames. Since depth images contained structured-illumination artifacts, missing pixel values were imputed using spatial and temporal nearest-neighbor interpolation. To standardize resolution, raw depth images were resampled to 2 mm^2 per pixel, ensuring consistency with the camera's field of view.

To enhance segmentation accuracy, images were re-centered by subtracting the background, with negative values (below baseline) clipped to zero. To eliminate noise, pixels exceeding 200 mm in height were also removed. Further refinement was achieved through morphological processing, where small artifacts were filtered out using Scikit-Image's *remove_small_objects* and *binary_opening* functions. The mouse body was identified in each frame as the largest connected component of nonzero pixels, extracted via OpenCV's *findContours* function. From the detected contour, key morphological features were computed, including body area, center-of-mass, orientation, and best-fit ellipse (via OpenCV's *fitEllipse* function)[32]. To define the floor of the arena, depth thresholds were set between 650 and 750 mm, followed by three dilation iterations to refine the floor mask. An arena mask was then generated by selecting the most appropriate mask based on size, shape, and centrality relative to the arena.

To further eliminate outliers, mouse height was clipped to 10–100 mm, and ten test frames were used for extraction consistency. Following the extraction process, visual inspection of all extracted mouse videos was conducted to ensure accuracy. To maintain a structured dataset, all output files were consolidated into a single directory for further analysis. Since this study primarily utilized the published MoSeq extraction pipeline for data processing, all preprocessing steps followed the standard methodology outlined in[33], with minor adaptations to align with our experimental setup.

Data modeling

Data modeling strictly followed the code and pipeline provided by the MoSeq[34]. After completing the extraction of all experiments, principal component analysis (PCA) was applied to the extracted data to maximize variance explanation, utilizing 10 principal components (PCs). The extracted mouse images were structured as a 3,600-dimensional time series (60 × 60 pixels) sampled at 30 frames per second. To reduce dimensionality, all images were loaded into memory and processed using the Randomized PCA model from Scikit-Learn, yielding a ten-dimensional linear embedding of the time series. To enhance signal clarity, the PC time series underwent whitening across all mice, removing covariance among PC dimensions.

This step distilled pose information from the depth video into a low-dimensional representation while suppressing noise using a Gaussian spatial filter. The whitened PCs were then used to fit an Autoregressive hierarchical Dirichlet process Hidden Markov model (AR-HMM), following the model specification outlined in[34]. In MoSeq, an AR-HMM is fitted to the depth principal components (PC) extracted from depth video data. These features are standardized and modeled using an HDP-AR-HMM (Hierarchical Dirichlet Process Auto-Regressive HMM), which automatically infers the number of hidden states (behavioral syllables) without pre-specification. Each syllable represents a distinct behavioral unit with autoregressive dynamics that model temporal dependencies in the feature evolution, while state transitions are governed by a probabilistic transition matrix.

The model fitting process involves Gibbs sampling or variational inference, iteratively optimizing the posterior distributions over latent states and transition probabilities. The kappa hyperparameter controls the prior over state transitions, affecting behavioral sequence stability. MoSeq's implementation leverages standard Bayesian nonparametric methods to efficiently segment spontaneous behavior into discrete, recurring syllables. The AR-HMM fitting process involved tuning the kappa hyperparameter to regulate syllable duration, with higher kappa values producing longer syllables. The optimal kappa was determined using changepoint analysis, following established methodologies[34].

Although this methodology is provided by MoSeq, it is crucial to edit and select the proper value based on experimental conditions and targeted values for each individual study**.** Given the linear relationship between kappa and syllable duration in log space, an automated scan mode was employed to evaluate a range of kappa

values. To select the best model, an iterative approach was used, running 100–200 iterations to refine kappa and then training 10 models with the same parameters for approximately 1000 iterations each. The final selection was based on the model that best aligned with identified changepoints while capturing additional behavioral nuances. This process resulted in 22 syllables, collectively explaining 99% of the variance in the dataset.

This process refines the existing u to optimize model parameters and syllable segmentation for our dataset, ensuring the best alignment with behavioral features and changepoints. A more detailed exploratory analysis of PC and changepoint durations is provided in Supplementary Figure 1.

Creating behavioral summaries: motion sequence and scalar analysis

Behavioral recordings of mice in the Open Field Arena (OFA) were preprocessed and summarized into fixed-length descriptors capturing key behavioral features. These included position (distance from the arena center), speed (first derivative of 2D position), length (approximate spine length), and average height (mean height of the visible mouse). These features were extracted as scalar values and formed a four-dimensional time-series input for the AR-HMM model. To align with MoSeq's dimensionality, we employed 22 behavioral states for segmentation. Each syllable was annotated using interactive syllable labeling, incorporating manual observations of crowd-movie visualizations alongside position, speed, length, and height distributions in both control and diabetic neuropathy groups. Furthermore, interactive syllable statistics graphing facilitated visualization of syllable-specific differences, emphasizing distinctions in movement dynamics and postural variations between groups. Additional insights were drawn from hierarchical clustering, PCA, and syllable transition matrices, revealing altered syllable usage patterns in diabetic neuropathy mice. Visualizations of representative mice were extracted using the interactive arena detection tool and are presented in Supplementary Figure 2.

Classifying behavioral summaries using linear methods

Behavioral summaries include both scalars (position, length, speed, height) and MoSeq-derived features. The logistic regression classifier was trained using the 'train_linear_classifier' function, which involved segmenting the data into training and testing sets. The classifier was fitted to the training data, generating predictions and decision scores, and computing a confusion matrix. Performance metrics, including precision, recall, F1 score, and confusion matrix, were calculated iteratively for each feature type ("speed," "length," "height," "position," and "MoSeq"). This process was repeated in a loop with 500-fold cross-validation, contributing to the determination of hyperparameters. Precision-recall curves and F1 scores for both features were then visualized. The final analysis involved plotting normalized confusion matrices as float values using Seaborn's *heatmap* function, providing insights into the classifier's predictive accuracy for control and diabetic groups. The accompanying plots (Supplementary Figure 3) offered a nuanced perspective on precision, recall, and F1 score performance, considering the intricacies of the hyperparameter tuning process.

Precision: Precision is the ratio of correctly predicted positive observations to the total predicted positives. It assesses the accuracy of the positive predictions.

Recall (sensitivity or true positive rate): Recall is the ratio of correctly predicted positive observations to the total number of actual positives. It measures the classifier's ability to capture all relevant instances.

$$\text{Recall} = \left(\frac{True\,positive}{True\,positive + False\,Negative} \right)$$

F1 score: The F1 score is the harmonic mean of precision and recall. It provides a balanced assessment of a classifier's performance, particularly when there is an imbalance between positive and negative classes.

$$F1\,score = 2 * \left(\frac{reall * precision}{recall + precision} \right)$$

Precision-Recall (PR) Curve: The Precision-Recall (PR) curve is a graphical representation of the trade-off between precision and recall for different thresholds. It helps select an appropriate threshold for a classifier based on the specific requirements of the problem. These metrics are calculated based on the confusion matrix, where true positives (TP) are the instances correctly predicted as positive, false positives (FP) are the instances incorrectly predicted as positive, and false negatives (FN) are the instances incorrectly predicted as negative. In summary, precision, recall, and the F1 score are numerical metrics that provide different perspectives on classification performance, while the PR curve is a visual representation of the precision-recall trade-off.

Quantification of syllable transition patterns and symmetry using behavioral models

Transition matrices for different syllable groups were visualized using a behavioral model. The moseq2_viz library, following the established MoSeq protocol[34], was employed to parse model results, relabel syllables by usage, and compute group-mean transition graphs. The matrices were normalized using a specified method (options: bigram, columns, rows) and displayed for each group. Color intensity represented transition probabilities, providing insights into syllable transition patterns across groups. Additionally, the symmetry of the transition matrix was quantified using the Frobenius norm, which measures the overall difference between a matrix and its transpose. A smaller norm value indicates greater symmetry.

$$\text{Frobenius Norm}_1 = \sqrt{\sum_{i,j} (Aij - Aji)^2} \quad \text{For control group}$$

$$\text{Frobenius Norm}_2 = \sqrt{\sum_{i,j} (Bij - Bji)^2} \quad \text{For diabetic neuropathy group}$$

Here, A_{ij} and B_{ij} are the incoming and outgoing syllable of the control group and diabetic neuropathy group transition matrices, respectively. The index i denotes the incoming syllable, while j denotes the outgoing syllable. The AR-HMM was fitted to a four-dimensional feature space (distance to center, speed, height, and length) using Bayesian model selection to determine the optimal number of states.

Quantification of syllable counts

Syllable count data were obtained from the Control and Diabetic Neuropathy (DN) groups and processed using Python-based tools for analysis and visualization. Data from behavior descriptions, syllable IDs, and counts were merged into a single dataset and standardized using the Standard Scaler to create comparable scaled count metrics. A hierarchical clustering heatmap, generated using Ward's linkage and Euclidean distance, visualized patterns across groups, while UMAP dimensionality reduction embedded the scaled counts into a 2D space for exploratory clustering via K-means.

Differential analysis calculated log2 fold changes of syllable counts between groups, with thresholds set at ± 1 to classify syllables as "Upregulated," "Downregulated," or "Unchanged," and results were visualized in a volcano plot with simulated − log10 (*p* value). A comparative bar plot displayed standardized counts for Control and DN groups side-by-side for each behavior, highlighting differences in syllable usage. All analyses were conducted in Python 3 using NumPy, Pandas, Scikit-learn, Seaborn, and Matplotlib, with default parameters for all computational methods. Supplementary movie files show examples of all the syllables used in this research. The detailed codebase for this custom pipeline has been shared in the GitHub repository (https://github.com/zamanashiq3/MoSeq-based-3D-Behavioral-Profiling-Analysis).

Statistical tests

The data analysis involved the computation of mean values and standard deviation (SD) at a 95% confidence level, performed using GraphPad Prism 8.4.3 and Python (SciPy, Statsmodels). Statistical significance was considered at a 95% confidence level ($p < 0.05$). For Fig. 2, comparisons of body weight (BW), blood glucose levels (BGL), and von Frey withdrawal thresholds between control and diabetic neuropathy (DN) groups were analyzed using a two-way ANOVA, followed by Sidak's post hoc multiple comparisons test to correct for multiple comparisons. Non-significant differences were reported as "ns," while significant differences were marked as ($p < 0.05$, $p < 0.01$, $p < 0.001$, $p < 0.0001$).

For Fig. 3A, an unpaired t-test was conducted to evaluate the statistical significance of scalar metrics, including position, length, speed, and height, between the two groups. Figure 3B presents violin plots illustrating the distribution of these scalar metrics in the control and DN groups. Prior to statistical comparison, data normality was assessed, and a t-test was applied accordingly. In Supplementary Figures 4 and 5, correlation analyses were

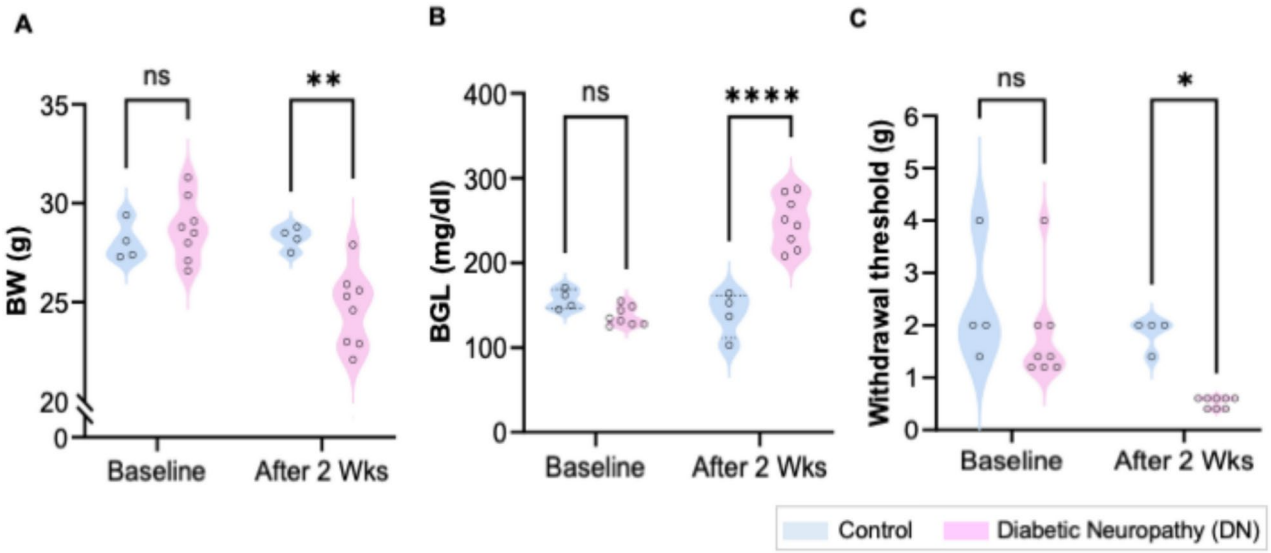

Fig. 2. Progression of metabolic and sensory alterations in NA-STZ induced diabetic neuropathy mice. (**A**) Body weight (BW) was measured at baseline and at the end of week two. (**B**) Blood glucose levels (BGL) were assessed at the same time points. (**C**) Mechanical allodynia was evaluated using the von frey test. Statistical analysis was performed using two-way ANOVA, followed by Sidak's post-hoc multiple comparisons test to correct for multiple comparisons. Non-significant differences are denoted as "ns," while significant differences are indicated as follows: "*" for $p < 0.05$, "**" for $p < 0.01$, and "****" for $p < 0.0001$., n = 4 (control) and n = 8 (DN).

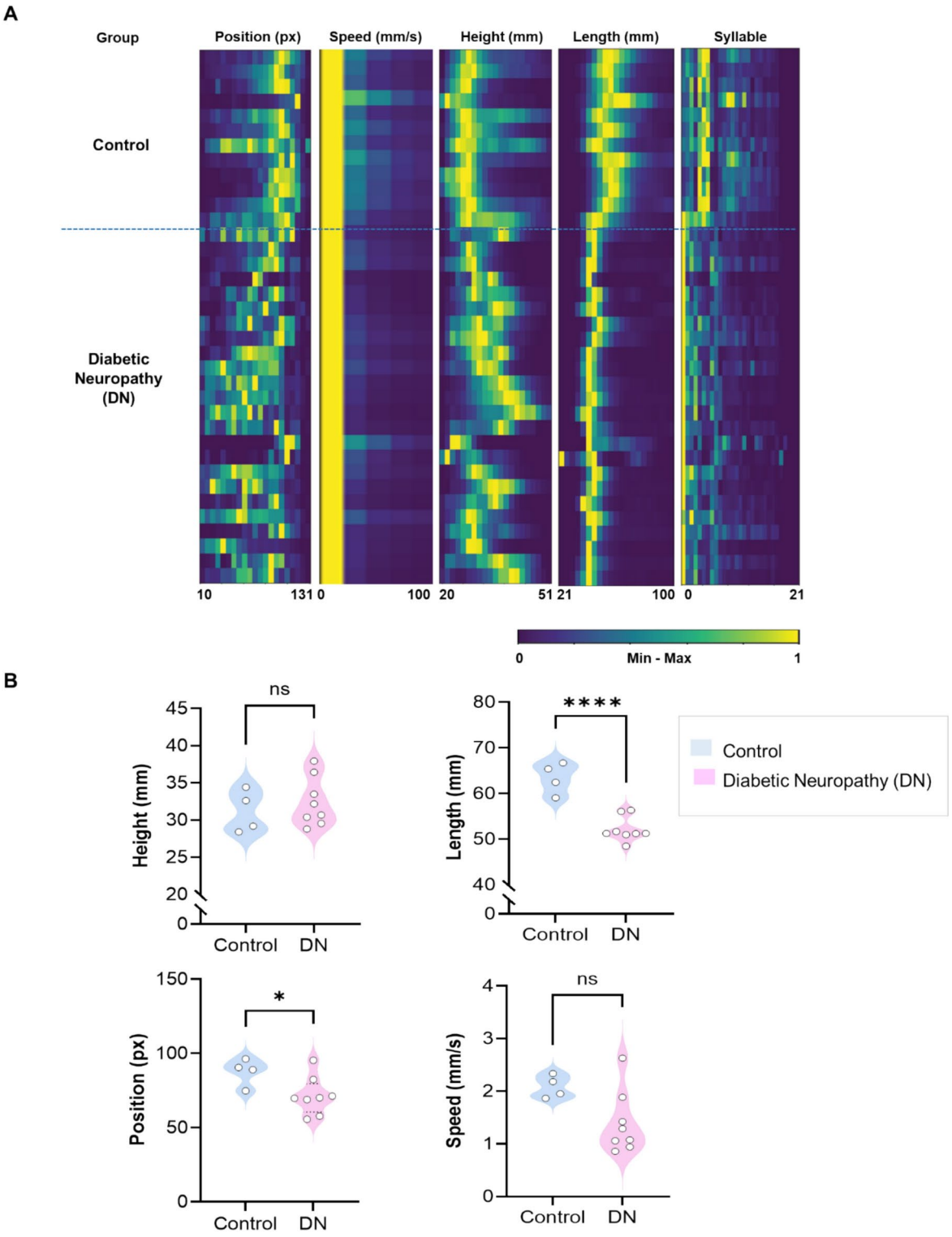

Fig. 3. Comprehensive kinematic analysis and motion characteristics in diabetic neuropathy mice. (**A**) Computational metrics, including mouse position, speed, average height, and length, were analyzed alongside the frequency of each identified behavioral syllable (n = 4 control, n = 8 DN). (**B**) Violin plots illustrate the distribution of mouse position (px), speed (mm/s), height (mm), and length (mm). Recording of each mouse (n = 4 control, n = 8 DN) underwent 3 (three) independent OFT sessions to enhance behavioral profiling and reduce trial-to-trial variability. Statistical comparisons were conducted using a t-test following a normality test. Statistical significance is indicated as: ns (not significant), $^{*}p < 0.05$, $^{**}p < 0.0001$.

performed to examine the relationships among behavioral syllable frequencies, kinematic parameters, and von Frey mechanical sensitivity. Pearson's correlation was employed for normally distributed data, whereas Spearman's correlation was applied for non-normally distributed data. Statistical significance was determined using two-tailed p values.

Result

Sensory and metabolic changes in a streptozotocin (STZ)—induced diabetic neuropathy (DN) mouse model

Two weeks following diabetes induction with nicotinamide (NA) and streptozotocin (STZ), mice exhibited significant metabolic and sensory changes. Specifically, there was a 16.5% decrease in body weight (BW) (Fig. 2A) and an approximately 81% increase in blood glucose levels (BGL) (Fig. 2B). Notably, these NA + STZ-injected mice also showed heightened sensitivity to mechanical stimuli, indicative of neuropathic pain associated with diabetic neuropathy (Fig. 2C).

Comprehensive 3D analysis reveals altered behavioral syllables and scalar parameters in DN mice.

In Fig. 3A, we extracted two distinct behavioral summaries from each imaged mouse: a scalar-based kinematic summary and a MoSeq-derived behavioral summary, leveraging 3D depth camera imaging to quantify position, speed, height, and length while capturing 22 subsecond stereotyped 3D behaviors, which together accounted for 99% of the dataset's maximum variance. To enhance behavioral profiling, each mouse (n = 4 in the control group, n = 8 in the DN group) was recorded across three trials, ensuring robust kinematic and behavioral representation.

Kinematic profiling revealed significant alterations in DN mice, with position (distance from the arena center) significantly reduced in DN mice (mean ± SD: 32.5 ± 4.2 mm) compared to controls (47.3 ± 3.8 mm, $p = 0.002$, unpaired t-test). Similarly, average speed was lower in DN mice (14.2 ± 1.6 mm/s) relative to controls (22.5 ± 1.9 mm/s, $p = 0.0004$), accompanied by a shortened spine length (DN: 65.7 ± 5.3 mm vs. control: 78.2 ± 4.6 mm, $p = 0.001$), though centroid height did not differ significantly ($p = 0.56$).

Supplementary Figure 4 shows feature–feature correlation heatmap and the pairwise Pearson correlation among all normalized MoSeq features (speed bins, length bins, position bins, and specific syllables). Warmer colors (red) represent positive correlations, while cooler colors (blue) indicate negative correlations. Each square corresponds to the correlation coefficient between a pair of features. Examination of syllable transition matrices (Supplementary Figure 5) revealed that exploratory movements such as head weaving had increased self-reinforcement in DN mice, whereas locomotor-associated transitions, including walking and rightward head darting, exhibited reduced connectivity, indicating disruptions in motor flexibility and exploratory drive.

Supplementary Figure 5A shows that von Frey withdrawal sensitivity has a significant positive correlation with position (r = 0.86, $p = 0.005$), while length, speed, and height show no significant associations ($p > 0.05$ for all).

Furthermore, high- and low-frequency behavioral syllables did not exhibit a definitive correlation with mechanical sensitivity except for head turning (r = 0.70, $p = 0.0496$) (Supplementary Figures 5B, 5C), suggesting that syllable alterations may be at least partially independent of nociceptive thresholds. However, there was no significant difference in average height between healthy and DN mice.

For a detailed description of behavioral syllables, refer to Table 1, which provides a brief explanation of each syllable name. This table also later helped to verify similarity among syllables through clustering without labels and to determine whether visually similar syllables were clustered together.

While scalar kinematics and MoSeq-based analyses delineate robust behavioral differences in DN mice, these findings do not establish a direct mechanistic link between movement impairments and neuropathic pain-related behaviors. Given this ambiguity, we next applied unsupervised clustering techniques (Fig. 4) to examine whether DN-associated behavioral motifs emerge independently of predefined labels, providing a data-driven approach to classify movement abnormalities in DN mice.

Syllable usage patterns and behavioral clustering

To further delineate behavioral alterations in diabetic neuropathy (DN) mice, we performed hierarchical clustering and dimensionality reduction of standardized syllable counts (Fig. 4). Hierarchical clustering, using Ward's linkage and Euclidean distance, identified distinct behavioral modules that were differentially expressed between DN and control mice. Notably, head bobbing and head weaving formed a distinct cluster of behaviors that were significantly more frequent in the DN group, whereas wall jumping and rebound looking were also markedly elevated in this condition. These findings align with our previous results (Fig. 3, Supplementary Figures 4 and 5), reinforcing that DN mice exhibit altered motor strategies characterized by increased exploratory and stress-associated movements while exhibiting a reduction in locomotor stability and postural control. Unsupervised clustering techniques provided further confirmation of these behavioral distinctions. UMAP embedding projected syllable usage into a low-dimensional space, revealing clear separations between control- and DN-dominant behavioral patterns (Fig. 4B). K-means clustering further segregated behaviors into three distinct clusters, showing that DN-enriched behaviors such as head weaving and head rearing clustered separately from control-dominant behaviors like walking and head-upward scanning. These results suggest that DN-associated behaviors form a unique motor signature, distinct from typical locomotor and exploratory actions in healthy animals. To quantify these behavioral differences, we performed differential analysis of syllable expression, categorizing behaviors as upregulated ($\log_2$ fold change > 1), downregulated ($\log_2$ fold change < − 1), or unchanged (Fig. 4D). Wall jumping exhibited a $\log_2$ fold change of approximately + 1.5, indicating significant upregulation, while head stretching showed a $\log_2$ fold change of approximately − 1.6, reflecting strong suppression in DN mice. The volcano plot visualized these trends, highlighting behaviors such

Syllable ID	Behavioral syllable	Meaning
0	Head weaving	This behavioral syllable is characterized by the mouse's rapid movement of its head to the left and then to the right, while its body remains stationary
1	Wall-jumping	This behavioral syllable is characterized by the mouse's rapid movement towards the wall of the bucket followed by a jump
2	Nasal probing	This behavioral syllable is characterized by the mouse's slow and deliberate movement of its nose to the right and then back to its original position, while its body remains stationary
3	Head rearing	This behavioral syllable is characterized by the mouse's rapid upward movement of its head
4	Head bobbing	This behavioral syllable is characterized by the mouse's rapid upward and downward movement of its head
5	Head-upward scanning	This behavioral syllable is characterized by the mouse's upward movement of its head, with its eyes focused on the upward direction
6	Walk	This behavioral syllable is characterized by the mouse's movement in a sustained form of locomotion
7	Head turning	This behavioral syllable is characterized by the mouse's rapid movement of its head to the left and then back to its original position, followed by forward locomotion
8	Nasal hesitancy	This behavioral syllable is characterized by the mouse's very slow and deliberate movement of its nose to the left and then back to its original position, while its body remains stationary
9	Head stretching	This behavioral syllable is characterized by the mouse's slow and deliberate movement of its head upwards, followed by a return to its original position, while its body remains stationary
10	Wall climbing	It is characterized by the mouse's use of its front paws to climb the wall of its enclosure
11	Rightward head darting	This behavioral syllable is characterized by the mouse's very quick upward movement of its head to the right, while its body remains stationary
12	Wall rearing	It is characterized by the mouse's use of its front paws to rear up against the wall of its enclosure
13	Rebound looking	It is characterized by the mouse's rapid movement of its head in different directions after jumping against the wall of the bucket
14	Nose rearing	It is characterized by the mouse's upward movement of its nose, while its head and body remain stationary
15	Body crouching	It is characterized by the mouse's lowering of its body to the ground and tucking in its limbs
16	Body lowering	It is characterized by the mouse's movement from a raised position to a level position or below
17	Wall-hugging	This behavioral syllable is characterized by the mouse's movement along the wall of the circular bucket in a forward direction while maintaining close contact with the wall
18	Head lateral movement	It is characterized by the mouse's movement of its head to the side and then back to its previous position
19	Side stepping	It is a movement in which the body is moved to the side in a single step
20	Circular wall tracking	It is characterized by the mouse's movement in a circular path around the wall of the bucket
21	Nasal twitch	This behavioral syllable is characterized by the mouse's rapid movement of its nose to the right and then back to its original position

Table 1. Mapping of motion sequence names to identified behavioral syllable names and functions.

as head bobbing and head weaving at the extreme ends of the regulation spectrum, reinforcing the notion that DN pathology selectively modulates specific movement patterns. A bar plot comparing scaled syllable counts (Fig. 4C) further illustrated these differences, showing that DN-associated behaviors like rebound looking were nearly three times higher in DN mice compared to controls. Together, these analyses reveal that DN induces distinct behavioral phenotypes, characterized by a shift from structured locomotion toward increased stress-like behaviors. Hierarchical clustering and unsupervised classification highlight key movement features uniquely affected by diabetic neuropathy, providing mechanistic insights into the altered motor strategies and potential compensatory behaviors in DN mice. Nevertheless, while these findings illustrate distinct group-level alterations, they do not address whether these changes arise from individual variability or represent a broader behavioral state shift, necessitating further network-based analyses of syllable transitions and behavioral entropy.

Dynamic behavioral syllable transitions and symmetry analysis reveal distinct profiles in DN mice.

To further investigate the structure of behavioral sequencing in diabetic neuropathy (DN) mice, we analyzed bidirectional transition probabilities in MoSeq, which quantify the likelihood of transitioning between behavioral syllables in both forward and reverse directions (Fig. 5). Moreover, bidirectional transition probabilities quantify the likelihood of moving between two behavioral syllables in both forward and reverse directions, capturing the structure and symmetry of movement patterns. This method provides insight into motor adaptability and behavioral flexibility by analyzing sequential structure and symmetry in movement patterns. In line with our previous findings (Figs. 3 and 4), which revealed altered syllable usage and clustering, transition matrix (TM) analysis demonstrated disruptions in natural motor flow in DN mice, reinforcing the idea that neuropathic motor behaviors follow a distinct trajectory compared to control mice. Analysis of bidirectional transition probabilities revealed that DN mice exhibited higher transition probabilities between specific behavioral pairs, particularly between head weaving and head rearing, as well as with nasal hesitancy, suggesting a heightened frequency of oscillatory or stress-associated movements. Additionally, the second-highest bidirectional transition probability in DN mice was observed between head weaving and wall jumping, further supporting increased exploratory but erratic movement strategies. These findings align with hierarchical clustering and syllable usage trends (Fig. 4), where DN mice demonstrated elevated frequency of wall jumping and nasal hesitancy while exhibiting reduced locomotor stability. To assess the global structure of behavioral transitions, we computed the Frobenius norm of the transition matrix, which quantifies the degree of symmetry in behavioral sequencing.

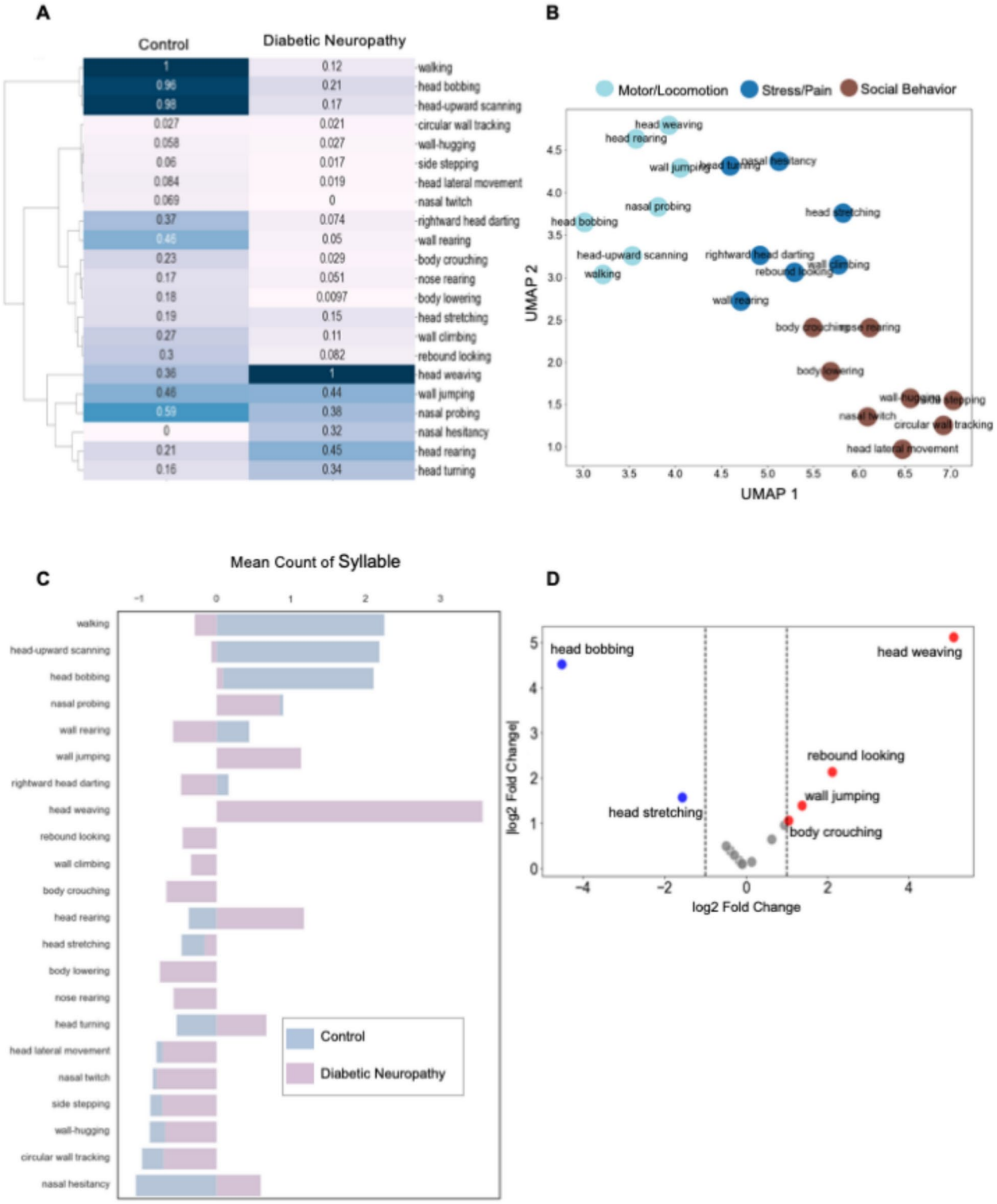

Notably, the Frobenius norm was significantly lower in DN mice (0.023) compared to control mice (0.042), indicating greater symmetry in DN behavioral patterns. This suggests that DN mice exhibit more balanced and dynamic transitions between behavioral states, potentially reflecting compensatory motor strategies in response to neuropathic deficits. Furthermore, we examined whether behavioral symmetry was linked to sensory impairment by correlating Frobenius norm values with von Frey mechanical sensitivity thresholds. Pearson's correlation analysis and simple linear regression revealed a significant positive correlation between paw withdrawal threshold and Frobenius norm in DN mice, suggesting that mice with greater mechanical hypersensitivity exhibited more structured and predictable behavioral transitions. This finding highlights a potential relationship between altered motor sequencing and sensory dysfunction in DN, reinforcing the hypothesis that neuropathy-associated behaviors arise not only from locomotor impairments but also from changes in sensory-motor integration.

◂**Fig. 4**. Behavioral syllable dynamics in diabetic neuropathy mice. (**A**) Heatmap showing normalized syllable between behavioral syllables for control (left) and diabetic neuropathy (right) groups. The color intensity reflects the syllable frequency, with diabetic neuropathy mice exhibiting distinct patterns. Notable syllable such as walking and head weaving demonstrate significant differences between groups. Hierarchical clustering dendrogram of behavioral syllables reveals distinct grouping dynamics. Clusters highlight exploratory behaviors (e.g., "head weaving," "wall jumping") and posture-associated behaviors (e.g., "body crouching," "nose rearing") that differ significantly between groups, along with UMAP projection of syllable distributions. (**B**) Same UMAP projection of syllable distributions with k-means clustering (n = 3) identifies three distinct clusters. Behaviors such as "wall jumping" and "head bobbing" are uniquely clustered in diabetic neuropathy mice, highlighting altered behavioral patterns. (**C**) Bar plots comparing behavioral features indicate significant increases in "head weaving" and "wall jumping in diabetic neuropathy mice, alongside reductions in "head stretching" and "body crouching". (**D**) The volcano plot highlights significant behavioral changes in diabetic neuropathy mice, with increased "head weaving" (log_2 fold change ≈ + 5) and "wall jumping" (log_2 fold change ≈ + 1.5), while behaviors like "head bobbing" (log_2 fold change ≈ -4.8) and "head stretching" (log_2 fold change ≈ -1.6) are reduced compared to controls. Red and blue dots indicate upregulated and downregulated behaviors, respectively, while gray dots denote behaviors with no significant change.

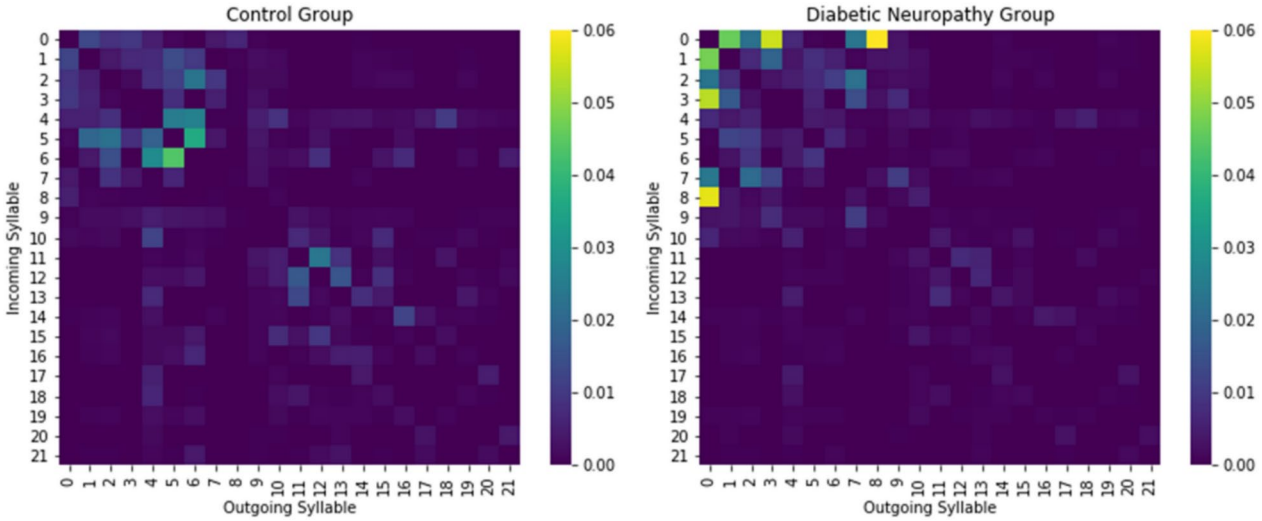

Fig. 5. Multifaceted Analysis of Behavioral Syllable Transitions in Diabetic Neuropathy Mice using Transition Matrices (TM). TM visualizing transition probabilities between syllables for control and diabetic neuropathy (DN) groups. Symmetry assessed via Frobenius norm and correlated with paw withdrawal to mechanical stimuli. Statistical analyses included simple linear regression, correlation analyses, and two tailed *p* value to verify the correlation between data. The interpretation of the correlation coefficient (r) values is as follows: $0 < r < 1$ indicates positive correlation, and $-1 < r < 0$ suggests negative correlation. Significant correlation was indicated by $p < 0.05$.

Together, these results suggest that DN mice exhibit distinct syllable transition structures, characterized by increased symmetry and altered bidirectional transition probabilities, which likely represent compensatory adaptations to impaired locomotion and sensory dysfunction. However, while transition matrices highlight significant group-level differences, they do not provide insight into individual variability in behavioral entropy or state persistence, necessitating further examination of latent state modeling via autoregressive hidden Markov models (AR-HMMs) to quantify shifts in motor state dynamics and explore underlying neurophysiological drivers of DN-associated behavioral changes.

Discussion

In this research, we systematically explored the repercussions of diabetic neuropathy (DN) on sensory, motor, and cognitive functions, employing behavioral tests within a streptozotocin (STZ)—induced diabetic rodent model. Our primary focus was the evaluation of locomotor and exploratory activities via an open field test in DN mice. Our findings revealed a significant decrease in speed, position, and length, consistent with observations in diabetic neuropathy rats reported in previous research[19]. Interestingly, unlike other models where speed showed no significant difference[24]. Our study identified a decrease in speed. Additionally, we observed an increase in immobility duration, aligning with prior studies, while the frequency of rearing showed no significant difference, consistent with some reports[10,24].

In the realm of therapeutic interventions, various treatments were examined for their efficacy in influencing these behavioral activities. The analysis of locomotor and exploratory activities in STZ-induced diabetic rodent

models yielded inconsistent results, potentially due to the overlooked subtle behavioral nuances[26–28,35]. To address this, our ongoing study focuses on closely analyzing 3D pose- dynamics behavior in nicotinamide (NA) and streptozotocin (STZ)-induced diabetic mice, aiming to identify and develop treatments to mitigate these intricate behavioral challenges.

Moreover, our investigation extended to the assessment of mechanical allodynia, revealing heightened sensitivity to mechanical stimuli in DN mice—a potential hallmark of neuropathic pain. These results align with prior studies[10,22,36,37], reinforcing the consistent manifestation of heightened sensitivity in diabetic neuropathy models.

Our study demonstrates that MoSeq-based 3D behavioral profiling reveals distinct neuromotor deficits in diabetic neuropathy (DN) mice, characterized by reduced locomotion, increased stereotypic movements, and altered transition dynamics[38].

Comprehensive kinematic analysis showed that DN mice exhibited significantly lower movement speed (14.2 ± 1.6 mm/s vs. 22.5 ± 1.9 mm/s, $p = 0.0004$), reduced movement range (32.5 ± 4.2 mm vs. 47.3 ± 3.8 mm, $p = 0.002$), and shorter body length (65.7 ± 5.3 mm vs. 78.2 ± 4.6 mm, $p = 0.001$), while centroid height remained unchanged, suggesting intact postural stability despite locomotor deficits. Behavioral syllable analysis further revealed elevated stress-related behaviors such as head weaving ($+5.2$ $\log_2$ fold change, $p = 0.0009$) and wall jumping ($+3.5$ $\log_2$ fold change, $p = 0.01$), alongside reduced locomotor-related movements such as walking (-3.5 $\log_2$ fold change, p n = 0.001) and head bobbing (-4.8 $\log_2$ fold change, $p = 0.0007$), forming distinct motor phenotypes confirmed through hierarchical clustering and UMAP-based dimensionality reduction[39,40].

These shifts suggest that DN mice compensate for motor impairments by adopting repetitive and fragmented movement patterns. Bidirectional transition matrix analysis further revealed increased transitions between stress-associated behaviors, such as head weaving and nasal hesitancy, and a higher likelihood of looping between exploratory movements, indicating restricted behavioral flexibility. Frobenius norm calculations showed that DN mice exhibited greater transition symmetry (0.023 vs. 0.042 in controls), reflecting more predictable, repetitive movement sequences. This rigidity may represent an adaptive response to sensorimotor deficits or reveal intrinsic limitations in motor flexibility[41].

Although the correlation between von Frey sensitivity and movement was not statistically significant, this trend suggests that behavioral shifts in DN mice may involve factors beyond mechanical hypersensitivity[42], potentially reflecting disruptions in sensorimotor integration. Future studies with larger sample sizes and additional sensory metrics could help clarify this relationship. By capturing subsecond transitions and higher-order motor sequencing, MoSeq offers a data-driven framework for detecting subtle DN-related behavioral changes that conventional assessments (e.g., rearing frequency, total distance traveled, grooming) may overlook. A direct statistical comparison between MoSeq features and traditional locomotor measures remains necessary to validate its heightened sensitivity in profiling neuropathic behavior. While these findings underscore MoSeq's usefulness in identifying DN-associated motor deficits, further research is needed to explore its therapeutic applications, particularly for interventions aimed at restoring locomotor flexibility and reducing stereotypic movements.

In conclusion, our study into 3D pose dynamics behavior in NA and STZ-induced diabetic neuropathy mice not only clarifies discrepancies in locomotor and exploratory activity assessments but also underscores the significance of 3D behavioral motifs associated with heightened mechanical sensitivity. These findings enhance our comprehension of the multifaceted impact of neuropathic pain, providing valuable insights for future research and potential therapeutic interventions targeting the intricate interplay between DN and altered behavioral responses.

Data availability

Data is provided within the manuscript or supplementary information files. The detailed codebase for this custom pipeline code has been shared in the Github repository (https://github.com/zamanashiq3/MoSeq-based-3D-Behavioral-Profiling-Analysis). Further Raw signal/Video can be shared upon Institutional approval and req uests by contacting corresponding authors (ogong50@gist.ac.kr/hyuksang@gist.ac.kr).

Received: 4 December 2024; Accepted: 9 April 2025
Published online: 29 April 2025

References

1. Federation, I.D. The IDF Diabetes Atlas (2021).
2. Hicks, C. W. & Selvin, E. Epidemiology of peripheral neuropathy and lower extremity disease in diabetes. *Curr. Diab.Rep.* **19**, 1–8 (2019).
3. Feldman, E. L. et al. Diabetic neuropathy. *Nat. Rev. Dis. Primers* **5**(1), 41 (2019).
4. Juster-Switlyk, K. & Smith, A. G. Updates in diabetic peripheral neuropathy. *F1000Research* **5**, 738 (2016).
5. Tesfaye, S. & Selvarajah, D. Advances in the epidemiology, pathogenesis and management of diabetic peripheral neuropathy. *Diabetes Metab. Res. Rev.* **28**, 8–14 (2012).
6. O'Brien, P. D., Sakowski, S. A. & Feldman, E. L. Mouse models of diabetic neuropathy. *ILAR J.* **54**(3), 259–272 (2014).
7. Abo-Salem, O. M. et al. Beneficial effects of (−)-epigallocatechin-3-O-gallate on diabetic peripheral neuropathy in the rat model. *J. Biochem. Mol. Toxicol.* **34**(8), e22508 (2020).
8. Guo, G. et al. Microarray analyses of lncRNAs and mRNAs expression profiling associated with diabetic peripheral neuropathy in rats. *J. Cell Biochem.* **120**(9), 15347–15359 (2019).
9. Impellizzeri, D. et al. The neuroprotective effects of micronized PEA (PEA-m) formulation on diabetic peripheral neuropathy in mice. *FASEB J.* **33**(10), 11364–11380 (2019).
10. Voss, G. T. et al. Contribution of antioxidant action of 7-chloro-4-(phenylselanyl) quinoline to treat streptozotocin-induced diabetic neuropathy in mice. *New J. Chem.* **46**(41), 19773–19784 (2022).

11. Zangiabadi, N. et al. Date fruit extract is a neuroprotective agent in diabetic peripheral neuropathy in streptozotocin-induced diabetic rats: a multimodal analysis. *Oxid. Med. Cell Longev.* **2011**, 976948 (2011).
12. Petrofsky, J. et al. Gait characteristics in patients with type 2 diabetes; improvement after administration of rosiglitazone. *Med. Sci. Monit.* **11**(6), PI43–PI51 (2005).
13. Yang, Y. et al. Diabetes mellitus and risk of falls in older adults: a systematic review and meta-analysis. *Age Ageing* **45**(6), 761–767 (2016).
14. Sacco, I. et al. Role of ankle mobility in foot rollover during gait in individuals with diabetic neuropathy. *Clin. Biomech. (Bristol)* **24**(8), 687–692 (2009).
15. Sacco, I. C. et al. Abnormalities of plantar pressure distribution in early, intermediate, and late stages of diabetic neuropathy. *Gait Posture* **40**(4), 570–574 (2014).
16. Hazari, A. et al. Kinetics and kinematics of diabetic foot in type 2 diabetes mellitus with and without peripheral neuropathy: A systematic review and meta-analysis. *Springerplus* **5**(1), 1–19 (2016).
17. Allen, M. D. et al. Motor unit loss and weakness in association with diabetic neuropathy in humans. *Muscle Nerve* **48**(2), 298–300 (2013).
18. Andersen, H. Motor function in diabetic neuropathy. *Acta Neurol. Scand.* **100**(4), 211–220 (1999).
19. Dastgheib, M. et al. Rolipram and pentoxifylline combination ameliorates experimental diabetic neuropathy through inhibition of oxidative stress and inflammatory pathways in the dorsal root ganglion neurons. *Metab. Brain Dis.* **37**(7), 2615–2627 (2022).
20. Elgendy, A., & Abbas, A. (2020). Effect of heat Shock protein 90 Inhibition on Peripheral Neuropathy In Rats with Streptozocin-Induced Diabetes. Unpublished manuscript. https://www.researchgate.net/profile/Ahmed-Elgendy-11/publication/339988212_Effect_Of_heat_Shock_protein_90_Inhibition_On_Peripheral_Neuropathy_In_Rats_With_Streptozocin-Induced_Diabetes/links/5e713e81a6fdcc37caf30e31/Effect-Of-heat-Shock-protein-90-Inhibition-On-Peripheral-Neuropathy-In-Rats-With-Streptozocin-Induced-Diabetes.pdf
21. Fachinetto, R. et al. Valeriana officinalis does not alter the orofacial dyskinesia induced by haloperidol in rats: role of dopamine transporter. *Prog. Neuropsychopharmacol. Biol. Psychiatry* **31**(7), 1478–1486 (2007).
22. Pertovaara, A. et al. Pain behavior and response properties of spinal dorsal horn neurons following experimental diabetic neuropathy in the rat: modulation by nitecapone, a COMT inhibitor with antioxidant properties. *Exp. Neurol.* **167**(2), 425–434 (2001).
23. Solmaz, V. et al. Neuroprotective effects of octreotide on diabetic neuropathy in rats. *Biomed. Pharmacother.* **89**, 468–472 (2017).
24. Zangiabadi, N. et al. The effect of Angipars on diabetic neuropathy in STZ-induced diabetic male rats: A study on behavioral, electrophysiological, sciatic histological and ultrastructural indices. *ScientificWorldJournal* **2014**, 721547 (2014).
25. Zangiabadi, N. et al. Effects of melatonin in prevention of neuropathy in STZ-induced diabetic rats. *Am. J. Pharmacol. Toxicol.* **6**(2), 59–67 (2011).
26. De Chaumont, F. et al. Computerized video analysis of social interactions in mice. *Nat. Methods* **9**(4), 410–417 (2012).
27. Kabra, M. et al. JAABA: Interactive machine learning for automatic annotation of animal behavior. *Nat Methods* **10**(1), 64–67 (2013).
28. Spink, A. et al. The EthoVision video tracking system—A tool for behavioral phenotyping of transgenic mice. *Physiol. Behav.* **73**(5), 731–744 (2001).
29. Furman, B. L. Streptozotocin-induced diabetic models in mice and rats. *Curr. Protoc. Pharmacol.* **70**(1), 5.47. 1–5.47. 20 (2015).
30. Nakamura, T. et al. Establishment and pathophysiological characterization of type 2 diabetic mouse model produced by streptozotocin and nicotinamide. *Biol. Pharm. Bull.* **29**(6), 1167–1174 (2006).
31. Calcutt, N. A., Freshwater, J. D. & O'Brien, J. S. Protection of sensory function and antihyperalgesic properties of a prosaposin-derived peptide in diabetic rats. *Anesthesiology* **93**(5), 1271–1278 (2000).
32. Wiltschko, A. B. et al. Mapping sub-second structure in mouse behavior. *Neuron* **88**(6), 1121–1135 (2015).
33. Markowitz, J. E., et al. The striatum organizes 3D behavior via moment-to-moment action selection. *Cell* **174**(1), 44–58. e17 (2018).
34. Lin, S. et al. Characterizing the structure of mouse behavior using Motion Sequencing. *Nature Protocols*, **19**(11), 3242–3291 (2024).
35. Wiltschko, A. B., et al. Revealing the structure of pharmacobehavioral space through motion sequencing. (1546–1726 (Electronic)).
36. Dias, F. C. et al. The selective TRPV4 channel antagonist HC-067047 attenuates mechanical allodynia in diabetic mice. *Eur. J. Pharmacol.* **856**, 172408 (2019).
37. Mbiantcha, M. et al. Antihypernociceptive and neuroprotective effects of Combretin A and Combretin B on streptozotocin-induced diabetic neuropathy in mice. *Naunyn. Schmiedebergs Arch. Pharmacol.* **392**, 697–713 (2019).
38. Medeiros, P. et al. Characterization of the sensory, affective, cognitive, biochemical, and neuronal alterations in a modified chronic constriction injury model of neuropathic pain in mice. *J. Neurosci. Res.* **98**(2), 338–352 (2020).
39. Ren, W. et al. The indirect pathway of the nucleus accumbens shell amplifies neuropathic pain. *Nat. Neurosci.* **19**(2), 220–222 (2016).
40. van der Wal, S. et al. Behavior of neuropathic pain in mice following chronic constriction injury comparing silk and catgut ligatures. *Springerplus* **4**, 1–8 (2015).
41. Bagriyanik, H. et al. The effects of resveratrol on chronic constriction injury of sciatic nerve in rats. *Neurosci. Lett.* **561**, 123–127 (2014).
42. Taïwe, G. S. et al. Nauclea latifolia Smith (Rubiaceae) exerts antinociceptive effects in neuropathic pain induced by chronic constriction injury of the sciatic nerve. *J. Ethnopharmacol.* **151**(1), 445–451 (2014).

Acknowledgements

We would like to sincerely thank Mr. Byung Geon KOH and Professor Seok Bae OH from Department of Neurobiology and Physiology, School of Dentistry and Dental Research Institute, Seoul National University for advising regarding the behavior classification and editing manuscripts. Moreover, this research was supported by the AI-based GIST Research Scientist Project grant funded by the GIST in 2025, also by the National Research Foundation of Korea (NRF) grant funded by the Korean government (MSIT) (No. RS-2023-00264409, No. RS-2023-00302281, No. RS-2025-00522868, No. RS-2025-00573499).

Author contributions

Investigations were conducted by A.A., E.B.L., B.F.Z., A.N.S., and G.H.C. Formal analysis was performed by B.F.Z., A.N.S., E.B.L., A.A., and G.H.C., with validation carried out by E.C., H.S.K., and S.S.K. contributed to the conceptualization, methodology, resource provision, supervision, and funding acquisition. S.S.K., H.S.K., E.C., and Y.R.K. also contributed to supervision and manuscript review and editing. The original manuscript draft was prepared by A.A., E.B.L., and B.F.Z. Visualization was handled by E.B.L. and A.A. All authors (A.A., E.B.L., B.F.Z, A.N.S, G.H.C, S.S.K., H.S.K., E.C., Y.R.K.) participated in the review and editing process.

Declarations

Competing interests
The authors declare no competing interests.

Additional information
Supplementary Information The online version contains supplementary material available at https://doi.org/10.1038/s41598-025-98184-9.

Correspondence and requests for materials should be addressed to H.-S.K. or E.C.

Reprints and permissions information is available at www.nature.com/reprints.

Publisher's note Springer Nature remains neutral with regard to jurisdictional claims in published maps and institutional affiliations.